

Coulomb-nuclear dynamics in the weakly-bound ^8Li breakup

B. Mukeru,¹ J. Lubian,² and Lauro Tomio³

¹*Department of Physics, University of South Africa, P.O. Box 392, Pretoria 0003, South Africa*

²*Instituto de Física, Universidade Federal Fluminense, Niterói, RJ, 24210-340, Brazil*

³*Instituto de Física Teórica, Universidade Estadual Paulista, 01140-070 São Paulo, SP, Brazil*

A detailed study of total, Coulomb and nuclear breakup cross sections dependence on the projectile ground-state binding energy ε_b is presented, by considering the $^8\text{Li}+^{12}\text{C}$ and $^8\text{Li}+^{208}\text{Pb}$ breakup reactions. To this end, apart from the experimental one-neutron separation energy of ^8Li nucleus ($\varepsilon_b = 2.03$ MeV), lower values of ε_b down to $\varepsilon_b = 0.01$ MeV, are also being considered. It is shown that all breakup processes become peripheral as $\varepsilon_b \rightarrow 0.01$ MeV, which is understood as due to the well-known large spacial extension of ground-state wave functions associated to weakly-bound projectiles. The Coulomb breakup cross section is found to be more strongly dependent on ε_b than the nuclear breakup cross section, such that the Coulomb breakup becomes more significant as ε_b decreases, even in a naturally nuclear-dominated reaction. This is mainly due to the long-range nature of the Coulomb forces, leading to a direct dependence of the Coulomb breakup on the electromagnetic transition matrix. It is also highlighted the fact that the nuclear absorption plays a minor role for small binding when the breakup becomes more peripheral.

Keywords: Nuclear fusion reactions; Cross sections; halo nuclei; ^8Li ; ^{208}Pb ; ^{12}C

PACS numbers: 24.10.Eq, 24.10.-i

I. INTRODUCTION

In the breakup of weakly-bound projectiles against heavy nuclei targets, a relevant phenomenon which has been investigated is the Coulomb-nuclear dynamics, such that considerable efforts have been made to understand the role of Coulomb-nuclear interference and the dynamics of fragments absorption in the breakup process. The established studies in this matter with the corresponding most relevant works can be found in Refs. [1–3]. For other complementary studies done in past two decades on the Coulomb-nuclear dynamics involving weakly-bound projectiles, with particular interest to our present investigation, we select the Refs. [4–12], as well as more recent works (among which we include contributions by some of us) in Refs. [13–22]. Despite the advances verified by these studies, the question on how both Coulomb and nuclear forces interfere to produce a total breakup remains far from being fully established. Some of the challenges emanate from the fact that, in a Coulomb-dominated reaction, small contribution of the nuclear breakup does not automatically imply insignificant Coulomb-nuclear interference [23–27]. It could be interesting to verify what happens in nuclear-dominated reactions.

In view of the long-range nature of Coulomb forces, a low breakup threshold is expected to lead to peripheral collisions, where the Coulomb breakup prevails over the nuclear breakup. In this peripheral region, the Coulomb breakup cross section depends on the projectile structure through the electromagnetic matrix elements of the projectile. Although not a general rule, according to the Coulomb dissociation method [28–31], the breakup cross section is simply the product of the reaction parameters and the projectile dipole electric transition probability. As the binding energy decreases, the reaction

becomes more peripheral, with the ratio between the Coulomb breakup cross section to the nuclear counterpart being expected to rise significantly, regardless the target mass. Intuitively, in this case, one would expect that the total breakup cross section becomes comparable to the Coulomb one, owing to both dynamic and static breakup effects. From the fact that lower is the ground-state binding, longer is the tail of the associated wave function, the nuclear forces are fairly stretched beyond the projectile-target radius. Therefore, for a projectile with very weak binding energy, even the nuclear breakup can be assumed to be a peripheral phenomenon, with the Coulomb-nuclear interference becoming stronger in the peripheral region.

The dependence of various reaction observables on the projectile ground-state binding energy has been studied recently in Refs. [32–37], in which different projectiles with different binding energies have been considered. One of the drawbacks being that all the projectiles do not have the same ground-state structure, mass and charge. Among other ways to circumvent such shortcomings, at least theoretically, one could artificially consider different binding energies for the same projectile (i.e., with nucleon-number A and charge Z unchanged), within an approach that has been adopted for instance in Refs. [34–37]. Even though a given nucleus has fixed ground-state energy, this is a convenient theoretical approach to unambiguously establish the dependence of the reaction observables on the projectile binding energy.

Another important aspect in breakup dynamics, relies on possible effects on other reaction observables, such as on fusion cross sections. While it is widely understood that the complete fusion suppression strongly depends on the projectile breakup threshold (see Ref. [38], for recent related studies), strong charge clustering has re-

cently been identified as the main factor responsible for such suppression, in the breakup of ^8Li on a heavy target [39]. Some behavior in the breakup of this nucleus, has also been reported in Refs. [40, 41]. Unlike several other loosely bound nuclei (such as ^8B , $^{6,7}\text{Li}$, and ^{11}Be), not much has been reported on the breakup dynamics of the ^8Li nucleus.

In view of the above discussion, we are motivated to study the breakup of ^8Li nucleus, within a model in which a valence neutron (n) is loosely bound to the ^7Li nucleus by a binding energy $\varepsilon_b = 2.03$ MeV [42], by considering the light and heavy targets ^{12}C and ^{208}Pb . The present study on the $^8\text{Li}+^{208}\text{Pb}$ breakup reaction is also extending a previous recent analysis for this reaction done in Ref. [37], where a critical angular momentum for complete fusion was also considered. We are particularly interested in analyzing the dependence of the resulting total, Coulomb and nuclear breakup cross sections, as well as the Coulomb-nuclear interference, on the projectile ground-state binding energy, in order to test the validity of the assumptions presented in the previous paragraphs. Within a more detailed investigation, we expect to show that for a much weaker projectile binding energy, the Coulomb breakup becomes dominant regardless the target mass, and the nuclear breakup becomes relatively peripheral, leading to a peripheral Coulomb-nuclear interference. Since both Coulomb and nuclear breakup cross sections increase with the decrease of the binding energy, a clear separation of their effects is not a simple task. The choice of ^{12}C and ^{208}Pb as the targets is motivated by the fact that, in the former case, the reaction should be dominated by the nuclear breakup, whereas it is dominated by Coulomb breakup in the latter case. In fact, ^{12}C was also used in Ref. [26], as a reference target when studying the ^{11}Be Coulomb dissociation on ^{208}Pb target. In our approach to obtain the corresponding total, Coulomb and nuclear breakup cross sections, we adopt the Continuum Discretized Coupled Channels (CDCC) formalism [43], with the Fresco code [44] being used for the numerical solutions.

The next sections are organized as follows: Sect. II provides some details on the model approach, with a summary of the CDCC formalism. Sect. III contains the main results for elastic and breakup cross sections, together with our analysis on the Coulomb-nuclear interference and possible absorption contributions. Finally, the Sect. IV presents a summary with our conclusions.

II. FORMALISM AND COMPUTATIONAL APPROACH

A. Brief description of the CDCC formalism

As mentioned in the introduction, in our numerical approach we use the CDCC formalism, in which we model the projectile ^8Li as ^7Li core nucleus, to which a neutron is loosely bound with ground-state energy $\varepsilon_b = 2.03$ MeV.

This state is defined in the core-neutron centre-of-mass (c.m.) by $n = 1$, $\ell_0 = 1$, $\tilde{j}_0^\pi = 2^+$ quantum numbers, where n stands for the radial state, ℓ_0 the orbital angular momentum and \tilde{j}_0^π the projectile total angular momentum with parity π . It is obtained by applying the usual spin-orbit coupling $\tilde{j}_0 = \ell_0 + \mathbf{1}/2$; $\tilde{j}_0 = \mathbf{j}_0 + \mathbf{I}_c$, with the core spin $I_c = 3/2$. In addition to the ground state, an excited bound state with energy $\varepsilon_{\text{ex}} = 0.98$ MeV (located in the $\tilde{j}_0^\pi = 1^+$ state [42]) was also considered in our coupling scheme. We would like to emphasize that we are not considering possible core excitations in our calculations.

In this formalism, we first consider the expansion of the three-body wave function on the projectile internal states. After that, by introducing the three-body expansion into the corresponding Schrödinger equation, a one-dimensional radial set of coupled differential equations can be derived for the radial wave-function components $\chi_\alpha^{LJ}(R)$, in terms of the projectile-target c.m. coordinate R , which is given by

$$\left[-\frac{\hbar^2}{2\mu_{pt}} \left(\frac{d^2}{dR^2} - \frac{L(L+1)}{R^2} \right) + U_{\alpha\alpha}^{LLJ}(R) \right] \chi_\alpha^{LJ}(R) + \sum_{\alpha' L' (\alpha' \neq \alpha)} U_{\alpha\alpha'}^{LL'J}(R) \chi_{\alpha'}^{L'J} = (E - \varepsilon_\alpha) \chi_\alpha^{LJ}, \quad (1)$$

where L is the orbital angular momentum associated with R , J is the total angular momentum, and μ_{pt} the projectile-target (pt) reduced mass. The total energy is given by E , with ε_α being the projectile bin energies. The index α appearing in the equation is representing a set of quantum numbers describing the projectile states, as given by $\alpha \equiv (i, \ell, s, j, I_c, \tilde{j})$, $i = 0, 1, 2, \dots, N_b$ (N_b = number of bins).

With the projectile-target potential given as a sum of the core-target (ct) and neutron-target (nt) terms, i.e., $U_{pt}(\mathbf{r}, \mathbf{R}) = U_{ct}(\mathbf{R}_{ct}) + U_{nt}(\mathbf{R}_{nt})$, where $\mathbf{R}_{ct} \equiv \mathbf{R} + \frac{1}{8}\mathbf{r}$ and $\mathbf{R}_{nt} \equiv \mathbf{R} - \frac{7}{8}\mathbf{r}$ (with \mathbf{r} being the projectile internal coordinate), the potential matrix elements $U_{\alpha\alpha'}^{LL'J}(R)$ in (1) are given by its Coulomb and nuclear parts, such that

$$U_{\alpha\alpha'}^{LL'J}(R) = \langle \mathcal{Y}_{\alpha L}(\mathbf{r}, \Omega_R) | V_{ct}^{Coul}(\mathbf{R}_{ct}) | \mathcal{Y}_{\alpha' L'}(\mathbf{r}, \Omega_R) \rangle + \langle \mathcal{Y}_{\alpha L}(\mathbf{r}, \Omega_R) | U_{ct}^{nucl}(\mathbf{R}_{ct}) | \mathcal{Y}_{\alpha' L'}(\mathbf{r}, \Omega_R) \rangle + \langle \mathcal{Y}_{\alpha L}(\mathbf{r}, \Omega_R) | U_{nt}^{nucl}(\mathbf{R}_{nt}) | \mathcal{Y}_{\alpha' L'}(\mathbf{r}, \Omega_R) \rangle, \quad (2)$$

where $\mathcal{Y}_{\alpha L}(\mathbf{r}, \Omega_R) \equiv [\hat{\Phi}_\alpha(\mathbf{r}) \otimes i^L Y_L^\Lambda(\Omega_R)]_{JM}$ is the direct product of the angular part of \mathbf{R} with the projectile channel wave function, $\hat{\Phi}_\alpha(\mathbf{r})$, which contains the square integrable discretized bin wave functions. The nuclear terms express the sums of real and imaginary parts. The former are responsible for the nuclear dissociation, whereas the latter accounts for the nuclear absorption. These nuclear terms are, respectively, given by $U_{ct}^{nucl}(\mathbf{R}_{ct}) = V_{ct}^{nucl}(\mathbf{R}_{ct}) + iW_{ct}^{nucl}(\mathbf{R}_{ct})$ and $U_{nt}^{nucl}(\mathbf{R}_{nt}) = V_{nt}^{nucl}(\mathbf{R}_{nt}) + iW_{nt}^{nucl}(\mathbf{R}_{nt})$, with the Woods-Saxon shape being adopted for both components. The diagonal coupling matrix elements $U_{\alpha\alpha}^{LLJ}(R)$, contain the monopole nuclear term in the

projectile-target c.m., which we denote by $V_{\beta_0\beta_0}^{LJ}(R) = \langle \Phi_{\beta_0}(\mathbf{r}) | U_{ct}^{nucl} + U_{nt}^{nucl} | \Phi_{\beta_0}(\mathbf{r}) \rangle$, where β_0 represents the set of ground-state projectile quantum numbers, $\beta_0 \equiv (k_0, \ell_0, s, j_0, I_c, \tilde{j}_0)$. The imaginary part accounts for the absorption in the projectile-target c.m. motion.

The separation of the Coulomb and nuclear interactions to obtain the Coulomb and nuclear breakup cross sections (σ_{Coul} and σ_{nucl} , respectively) remains a challenge in nowadays theories, making an accurate description of the Coulomb-nuclear interference a more tricky task. For that, in this work we resort to an approximate approach, as follows: The nuclear breakup cross sections, defined as σ_{nucl} , are obtained by including in the coupling matrix elements, the nuclear components of U_{ct} and U_{vt} potentials, plus the diagonal monopole Coulomb potential. On the other hand, the Coulomb breakup cross sections, defined as σ_{Coul} , are obtained by including in the matrix elements the Coulomb component of the projectile-target potential, i.e., $V_{ct}^{Coul}(R_{ct})$ (as $V_{nt}^{Coul} = 0$), plus the monopole nuclear potential. The total breakup cross sections σ_{tot} are obtained by including the full U_{pt} potential in the calculations.

Since the early works on Coulomb and nuclear breakup studies [4, 5], this approach has been widely adopted to study Coulomb and nuclear breakup cross sections, as one can follow from the review [45] (and references therein). In Ref. [20], where different methods are considered in order to decompose the total breakup into its Coulomb and nuclear components, this approach is also referred as *weak-coupling approximation*. Two methods emerged from their discussion, which they refer to as *method 1* and *method 2*. The weak-coupling approximation is very close to *method 1* for nuclear breakup, and close to *method 2* for Coulomb breakup. While this approximate procedure will not completely eliminate the ambiguities surrounding the separation of the total breakup cross section into its Coulomb and nuclear components (as also outlined in Ref.[20]), we believe that it is particularly justified in the present work, since by using the ^{12}C target, the breakup is naturally dominated by nuclear dissociation, whereas by using the ^{208}Pb target the breakup is dominated by Coulomb dissociation.

Once the matrix elements (2) are computed, the coupled Eq. (1) is solved with the usual asymptotic conditions, which for $k_\alpha \equiv \sqrt{(2\mu_{pt}/\hbar^2)(E - \varepsilon_\alpha)}$ is given by

$$\chi_\alpha^{LJ}(R) \xrightarrow{R \rightarrow \infty} \frac{i}{2} \left[H_\alpha^-(k_\alpha R) \delta_{\alpha\alpha'} - H_\alpha^+(k_\alpha R) S_{\alpha\alpha'}^{LL'J} \right], \quad (3)$$

where $H_\alpha^\mp(k_\alpha R)$ are the usual incoming (-) and outgoing (+) Coulomb Hankel functions [46], with $S_{\alpha\alpha'}(k_\alpha)$ being the scattering S-matrix elements. Due to the short-range nature of nuclear forces, the matrix elements corresponding to the nuclear interaction in Eq. (2) will vanish at large distances, $R \gg R_n$, where

$$R_n \equiv r_0(A_p^{1/3} + A_t^{1/3}) + \delta_R(\varepsilon_b) \equiv R_0 + \delta_R(\varepsilon_b) \quad (4)$$

determines the range of the nuclear forces (r_0 being the

nucleon size, with $r_0 A_p^{1/3}$ and $r_0 A_t^{1/3}$ the projectile and target sizes, respectively). The function $\delta_R(\varepsilon_b)$ is introduced to take into account the well-known effect which occurs in weakly-bound systems (low breakup thresholds), as in halo nuclei, in which the nuclear forces can be stretched beyond $R_0 = r_0(A_p^{1/3} + A_t^{1/3})$. The various breakup cross sections are obtained by using the relevant S-matrix, as outlined for example in Ref. [2].

At large distance ($R \rightarrow \infty$), Eq.(2) contains only the Coulomb interaction, which can be expanded as [47]

$$V^{Coul}(\mathbf{r}, \mathbf{R}) \xrightarrow{R \rightarrow \infty} 4\pi Z_t e \sum_{\lambda=0}^{\lambda_{\max}} \frac{\sqrt{2\lambda+1}}{R^{\lambda+1}} [\mathcal{O}_\lambda^\epsilon(\mathbf{r}) \otimes Y_\lambda(\Omega_R)]^0, \quad (5)$$

where $Z_t e$ is the target charge, with λ the multipole order truncated by λ_{\max} . $\mathcal{O}_\lambda^\epsilon(\mathbf{r})$ is the projectile electric operator, given by

$$\mathcal{O}_{\lambda\mu}^\epsilon(\mathbf{r}) = \left[Z_{ce} \left(-\frac{A_n}{A_p} \right)^\lambda \right] r^\lambda Y_\lambda^\mu(\Omega_r) = Z_\lambda r^\lambda Y_\lambda^\mu(\Omega_r), \quad (6)$$

where Z_{ce} is the charge of the projectile core, with Z_λ being defined as the effective charge. The projectile electric transition probability for the transition from the projectile ground-state to the continuum states can be obtained through $\mathcal{O}_\lambda^\epsilon(\mathbf{r})$ [48]. For excitation energies ε , the corresponding variation of the electric transition probability $B(E\lambda)$ can be written as

$$\frac{dB(E\lambda)}{d\varepsilon} = \frac{\mu_{cn}}{\hbar^2 k} \sum_{\tilde{j}} (2\tilde{j}+1) |\langle \Phi_{\beta_0}(\mathbf{r}) | \mathcal{O}_\lambda^\epsilon(\mathbf{r}) | \Phi_\beta(\mathbf{r}) \rangle|^2, \quad (7)$$

where (β) refers to the set of quantum numbers in the continuum states $\beta \equiv (k, \ell, s, j, I_c, \tilde{j})$, $k = \sqrt{2\mu_{cn}\varepsilon/\hbar^2}$, $k_0 = \sqrt{2\mu_{cn}|\varepsilon_0|/\hbar^2}$, with μ_{cn} the core-neutron reduced mass. By defining $\hat{l} \equiv \sqrt{2l+1}$ for general angular quantum numbers, from the above we obtain

$$\begin{aligned} \frac{dB(E\lambda)}{d\varepsilon} &= \frac{\mu_{cn}}{\hbar^2 k} \sum_{\tilde{j}} (2\tilde{j}+1) |\mathcal{F}_{\lambda,\tilde{j}}|^2, \quad \text{with} \quad (8) \\ \mathcal{F}_{\lambda,\tilde{j}} &\equiv \frac{1}{4\pi} Z_\lambda \hat{\ell}_0 \hat{\lambda}^2 \hat{j}_0 \hat{j} (-1)^{\ell_0 + \ell + s + j + j_0 + I_c + \tilde{j}} \\ &\times \begin{pmatrix} \ell & \lambda & \ell_0 \\ 0 & 0 & 0 \end{pmatrix} \begin{pmatrix} j & \lambda & j_0 \\ 0 & 0 & 0 \end{pmatrix} \begin{Bmatrix} s & \ell_0 & j_0 \\ \lambda & j & \ell \end{Bmatrix} \\ &\times \begin{Bmatrix} I_c & j_0 & \tilde{j}_0 \\ \lambda & \tilde{j} & j \end{Bmatrix} \int_0^\infty dr u_{k_0\ell_0}^{\tilde{j}_0}(r) r^\lambda u_{k\ell}^{\tilde{j}}(r), \end{aligned}$$

where $u_{k_0\ell_0}^{\tilde{j}_0}(r)$, and $u_{k\ell}^{\tilde{j}}(r)$ are the ground-state and continuum radial wave functions. The Eqs. (5)-(8) are indicating how the Coulomb breakup is being affected by the projectile structure.

B. Computational details

The energies and corresponding wave functions which appear in the set of coupled differential equations (1), for

the bound and continuum states of the ${}^7\text{Li}+n$ system, are obtained by considering a two-body Woods-Saxon potential as input, whose parameters are the same as in Ref. [49]. The depth V_0 of the central part of the potential was adjusted to reproduce the ground and excited bound-state energies. These parameters are summarized in Table I. Similarly, the other binding energies consid-

TABLE I: Woods-Saxon potential parameters for the projectile ($n-{}^7\text{Li}$) ground and excited bound-state energies.

j^π	V_0 (MeV)	r_0 (fm)	a_0 (fm)	V_{SO} (MeV/fm ²)	r_{SO} (fm)	a_{SO} (fm)
2^+	37.22	1.25	0.52	4.89	1.25	0.52
1^+	46.65	1.25	0.52	4.89	1.25	0.52

ered in this work are obtained by adjusting V_0 . The same ground-state potential parameters are adopted to calculate the corresponding continuum wave functions. With these potential parameters, we first calculate the electric transition probability $B(E1)$ variation with the excitation energy ε , given by Eq.(8), corresponding to the transition from the ground-state to continuum s - plus d -states, for the binding energies $\varepsilon_b = 0.01$ MeV, 1.0 MeV and 2.03 MeV. The results are shown in the upper panel of Fig.1. One notices that $B(E1)$ varies substantially for $\varepsilon_b = 0.01$ MeV as compared with values obtained for larger ε_b . These results highlight the strong dependence of the Coulomb breakup on the projectile internal structure, particularly in the asymptotic region. In this regard, it is also instructive to verify how the projectile root-mean-square radii $\sqrt{\langle r^2 \rangle}$ vary with the projectile ground-state binding energies. For that, we add the lower panel of Fig. 1, with the corresponding root-mean-square radii, obtained for the projectile ground-state $\Phi_{\beta_0}(\mathbf{r})$. As expected, the root-mean-square radii behavior is reflecting the large increasing of the wave function as the binding energy comes close to zero. Also, for $\varepsilon_b = 2.033$ MeV, we note that we obtain $\sqrt{\langle r^2 \rangle} = 2.39$ fm, in very close agreement with the corresponding values reported in Refs. [50] and [51] (respectively, $\sqrt{\langle r^2 \rangle} = 2.39 \pm 0.05$ fm and $\sqrt{\langle r^2 \rangle} = 2.37 \pm 0.02$ fm).

In order to evaluate the coupling matrix elements of Eq. (1), fragments-target optical potentials are needed. The ${}^7\text{Li}+{}^{12}\text{C}$ optical potential parameters were taken from Ref. [52], whereas the ${}^7\text{Li}+{}^{208}\text{Pb}$ optical potential parameters were obtained from the ${}^7\text{Li}$ global potential of Ref. [53], with the depth of the real part slightly modified to fit the elastic scattering experimental data. For the n -target optical potentials, we adopted the global potential of Ref. [54]. The CDCC limiting values of the model space parameters, used for the numerical solution of Eq.(1), are listed in Table II, for the two targets we are considering, ${}^{12}\text{C}$ and ${}^{208}\text{Pb}$, where ℓ_{max} is the maximum angular momentum between ${}^7\text{Li}$ and the neutron, λ_{max} is the maximum order of the potential multipole expansion, ε_{max} is the maximum bin energies, r_{max} is the

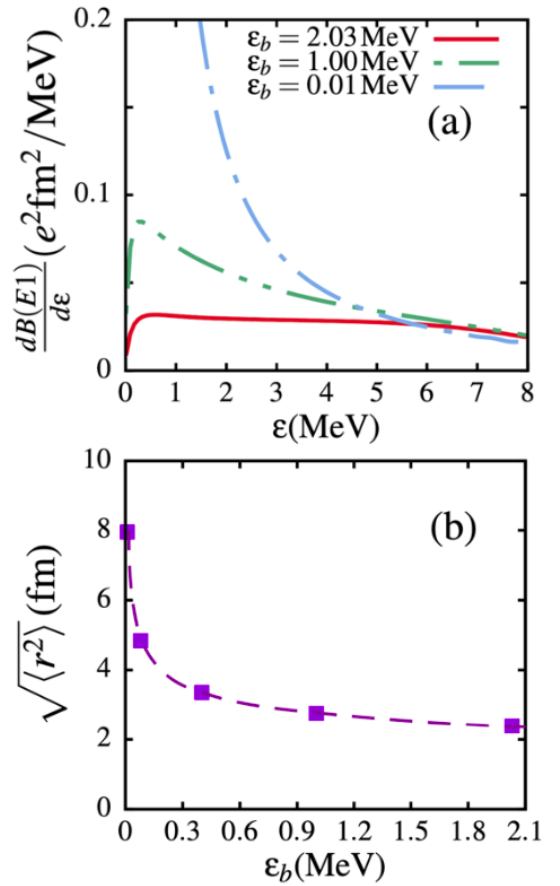


FIG. 1: In panel (a), considering three different ${}^7\text{Li}$ - n ground-state binding energies ε_b , it is shown how the derivative of the electric transition probability, given by (8), varies with the excitation energy ε , for transitions from ground to continuum s - plus d -states. In panel (b), the root-mean-square radii is shown as a function of the binding energy ε_b .

maximum matching radius for bin potential integration, L_{max} is the maximum angular momentum of the relative c.m. motion, and R_{max} is the maximum matching radius of the integration for the coupled differential equations, with ΔR the corresponding R -step size. The reported main values are found to give enough converged results for $\varepsilon_b \geq 0.4$ MeV. However, as we decrease the projectile binding energy, for $\varepsilon_b \leq 0.08$ MeV, to guarantee enough good convergence and precision of the results we found necessary to increase the maximum values for the projectile matching radius r_{max} , for the matching radius R_{max} , and for the relative angular momentum of the c.m. motion, L_{max} , correspondingly to each of the target. These values for smaller ε_b are shown within parenthesis, below the respective values obtained for larger ε_b . The adopted bin widths were, $\Delta\varepsilon = 0.5$ MeV, for s - and p -states, $\Delta\varepsilon = 1.0$ MeV, for f - and d -states and $\Delta\varepsilon = 1.5$ MeV for g -states.

TABLE II: Maximum model space parameters, for optimal numerical convergence of Eq. (1) for both ^{12}C and ^{208}Pb targets. The main reported values are for $\varepsilon_b \geq 0.4\text{MeV}$, with the corresponding ones within parenthesis for $\varepsilon_b \leq 0.08\text{MeV}$.

Target	ℓ_{\max}	λ_{\max}	ε_{\max}	r_{\max}	L_{\max}	R_{\max}	ΔR
	(\hbar)		(MeV)	(fm)	(\hbar)	(fm)	(fm)
^{12}C	3	3	6	80	300	300	0.08
				(100)	(1000)	(500)	
^{208}Pb	4	4	10	80	1000	600	0.03
				(100)	(10000)	(1000)	

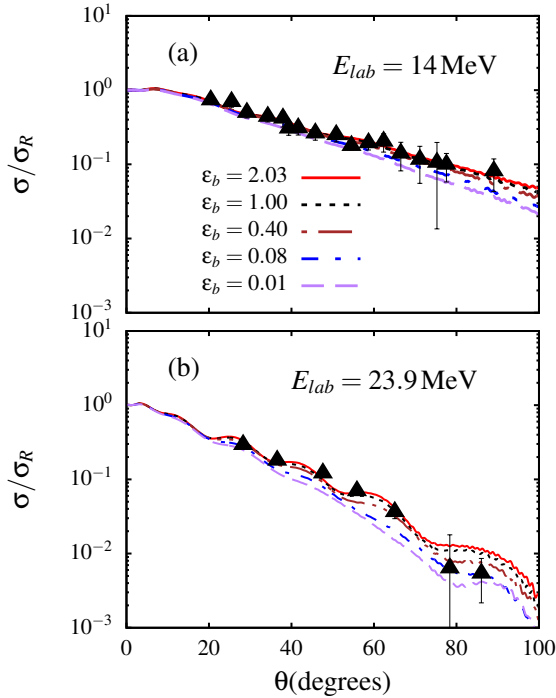


FIG. 2: $^8\text{Li}+^{12}\text{C}$ elastic scattering cross sections for the incident energies, $E_{lab} = 14\text{ MeV}$ and $E_{lab} = 23.9\text{ MeV}$. The model results are for different ^8Li binding energies ε_b (in MeV units), as indicated inside panel (a) for both panels. The available experimental data, converted to Rutherford σ_R units, are from Refs. [55] [panel (a)] and [52] [panel (b)], as indicated in the database reported in Ref. [56].

III. RESULTS AND DISCUSSION

A. Elastic scattering cross sections

We start the first part of this section by analyzing the dependence of the elastic scattering cross sections on the projectile ground-state binding energy. These cross sections are displayed in Fig. 2 for ^{12}C target; and in Fig. 3 for ^{208}Pb target, considering two incident energies. In both the cases, we assume different values of ε_b , from the experimental one down to 0.01 MeV. In the case of ^{12}C target, which is a nuclear-dominated reaction, from the

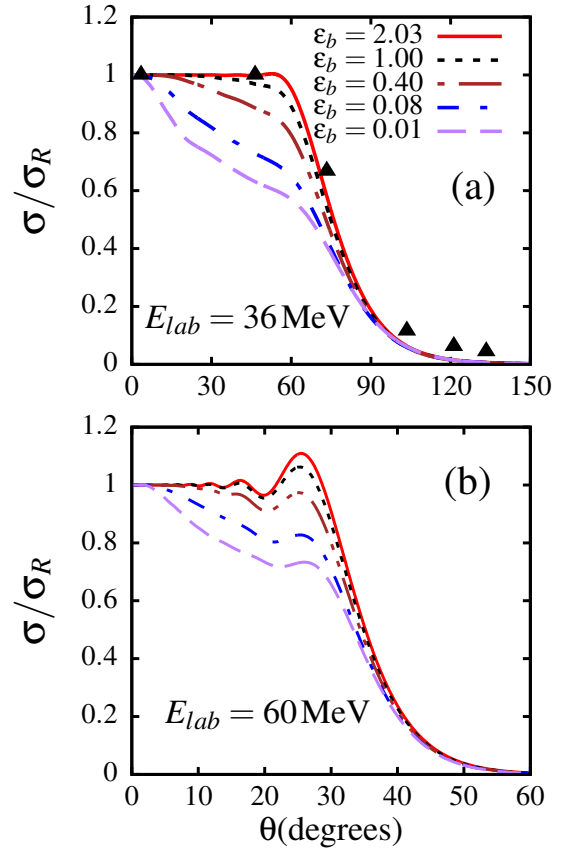


FIG. 3: $^8\text{Li}+^{208}\text{Pb}$ elastic scattering cross sections (in units of the Rutherford σ_R), obtained for the incident energies $E_{lab} = 36\text{ MeV}$ [panel (a)] and $E_{lab} = 60\text{ MeV}$ [panel (b)]. As in Fig. 2, the results are for the same set of ε_b (in MeV). From Ref. [57], we included in (a) the closest available experimental data, which are for $E_{lab} = 30.6\text{ MeV}$, as indicated in the database reported in Ref. [56].

results shown in Fig. 2 one can observe a weak dependence on ε_b in the range $0.4\text{ MeV} \leq \varepsilon_b \leq 2.03\text{ MeV}$, for both incident energies, $E_{lab} = 14\text{ MeV}$ [panel (a)] and 24 MeV [panel (b)]. However, it becomes relatively significant for $\varepsilon_b \leq 0.08\text{ MeV}$ [see panel (a)]. Also shown in Fig. 2 is that the experimental data are well reproduced by the model for both incident energies.

For the Coulomb-dominated reaction with ^{208}Pb , the results given in Fig. 3 for $E_{lab} = 36\text{ MeV}$ (a) and 60 MeV (b) are indicating strong dependence of the elastic scattering cross sections on all binding energies at forward angles (asymptotic region), where the Coulomb breakup is particularly dominant. However, at backward angles (short distance), where the nuclear breakup is expected to provide meaningful effects, the elastic cross sections become almost independent of the binding energy.

These results lead to a conclusion that, when the nuclear breakup is dominant or relatively significant, the effect of the binding energy on the elastic scattering cross section is rather small, whereas it is more pronounced

when the Coulomb breakup is dominant. Therefore, since a relatively significant effect for the ${}^8\text{Li} + {}^{12}\text{C}$ reaction is observed when $\varepsilon_b \leq 0.08$ MeV, it is possible that the ${}^8\text{Li} + {}^{12}\text{C}$ reaction is already dominated by the Coulomb breakup for $\varepsilon_b \leq 0.08$ MeV. As the binding energy decreases, the Coulomb breakup becomes dominant over its nuclear counterpart, as anticipated. It also follows that the probability of the projectile to fly on the outgoing trajectory unbroken decreases, diminishing the corresponding elastic scattering cross section. In the next section, we will look into this observation in more detail.

B. Breakup cross sections

The differential total, Coulomb and nuclear breakup cross sections, for the ${}^{12}\text{C}$ target, are depicted in Fig. 4, for $E_{lab} = 14$ MeV [(a)-(e) panels] and $E_{lab} = 24$ MeV [(f)-(j) panels]. As anticipated, in the case of nuclear-dominated reactions, for both incident energies, $d\sigma_{nucl}/d\Omega \simeq d\sigma_{tot}/d\Omega \gg d\sigma_{Coul}/d\Omega$ as $\varepsilon_b \rightarrow 2.03$ MeV, with $d\sigma_{Coul}/d\Omega \rightarrow 0$. However, it is interesting to notice that as ε_b decreases, the Coulomb breakup increases rapidly, such that for $\varepsilon_b \rightarrow 0.01$ MeV, $d\sigma_{nucl}/d\Omega \ll d\sigma_{Coul}/d\Omega \simeq d\sigma_{tot}/d\Omega$ at forward angles, for both incident energies. On the light of these results it follows that as the binding energy further decreases, the Coulomb breakup becomes more relevant, and comparable with the total breakup even in such a naturally nuclear-dominated reaction. This can be attributed to the fact that the breakup becomes more peripheral as ε_b decreases, where only Coulomb forces are available. Hence, the importance of the Coulomb breakup in this case relies mainly on the long-range behavior of the Coulomb forces, and on its direct dependence on the electromagnetic transition matrix elements, in agreement with our assessment in Sect. III A. Furthermore, these results show that the “nuclear-dominated reaction” concept may be relative to the projectile binding energy.

As the projectile binding energy varies from 2.03 MeV down to 0.01 MeV, one may wonder how relevant higher-order partial-waves (ℓ) are in the breakup process for such very low binding energy, particularly for heavy targets. In order to verify the importance of higher-order partial-waves in this case, we performed a convergence test of the total, Coulomb and nuclear differential breakup cross sections for ${}^{208}\text{Pb}$ target at $E_{lab} = 36$ MeV. The different breakup cross sections are shown in Fig. 5, as functions of the c.m. angle θ , for different maximum projectile internal angular momenta ℓ_{max} , and only for $\varepsilon_b = 0.01$ MeV and 2.03 MeV binding energies. As evidenced by the results in this figure, there is no meaningful difference between $\ell_{max} = 4$ and $\ell_{max} = 7$, regardless the binding energy. This implies that, by reducing the ground-state binding energy, the convergence of the breakup cross sections is not affected, in respect to the maximum core-neutron orbital angular momentum ℓ_{max} .

In Fig. 6, displays, the total, Coulomb and nuclear

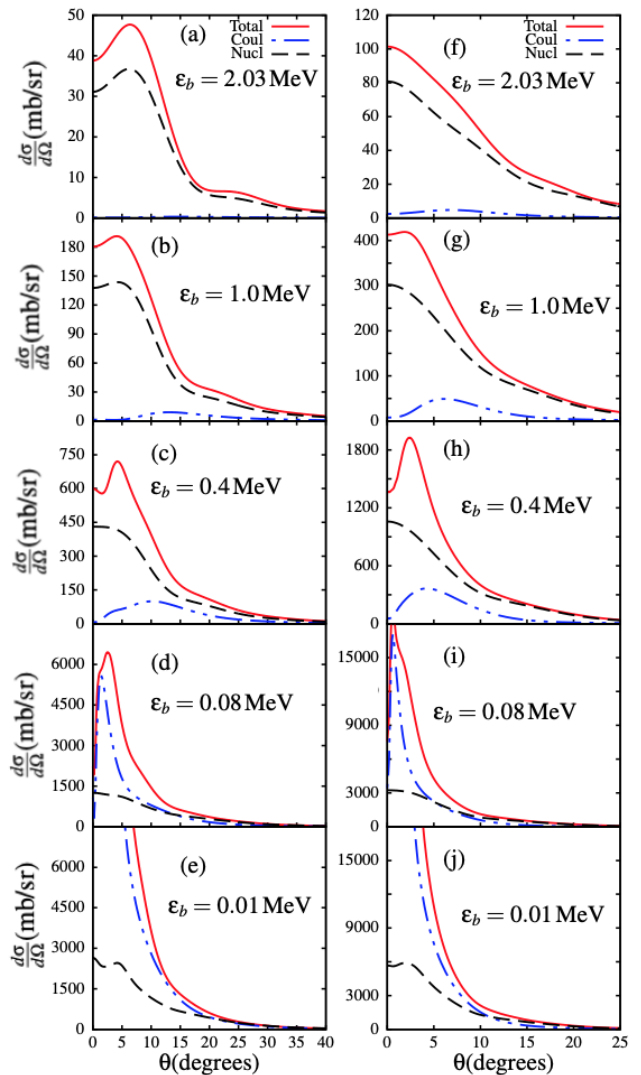


FIG. 4: For incident energies $E_{lab} = 14$ MeV (left column) and $E_{lab} = 24$ MeV (right column), with fixed different ε_b (shown inside the panels), the ${}^8\text{Li} + {}^{12}\text{C}$ angular distributions for the total, Coulomb and nuclear differential breakup cross sections $d\sigma/d\Omega$ (identified inside the upper panels) are shown as functions of the c.m. angle θ .

breakup angular cross-section distributions as functions of the c.m. angle θ , for the different binding energies ε_b , for ${}^8\text{Li} + {}^{208}\text{Pb}$ reaction. We first observe that as ε_b decreases, the peaks of $d\sigma_{tot}/d\Omega$ and $d\sigma_{Coul}/d\Omega$ are shifted to forward angles. In fact, for $\varepsilon_b \leq 0.08$ MeV, the peaks are located close to zero degree. This is a clear display of the peripheral nature of the breakup process as ε_b decreases. A careful look at this figure also indicates that as ε_b decreases, even the peak of $d\sigma_{nucl}/d\Omega$ is shifted to forward angles, which may suggest that even the nuclear breakup process becomes peripheral as $\varepsilon_b \rightarrow 0.01$ MeV. The peripherality of the nuclear breakup in this case, can be understood by considering the function $\delta_R(\varepsilon_b)$,

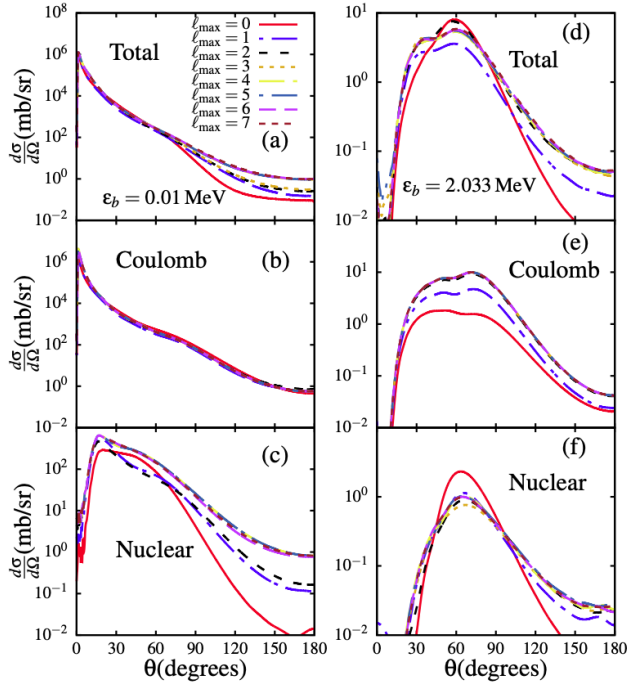


FIG. 5: Convergence sample results for the ${}^8\text{Li}+{}^{208}\text{Pb}$, total (upper frames), Coulomb (middle frames) and nuclear (bottom frames) breakup angular distributions, $d\sigma/d\Omega$, at $E_{lab} = 36$ MeV, considering different maximum projectile internal angular momenta ℓ_{max} (indicated in the upper-left frame). The left set [(a)-(c)] is for $\varepsilon_b = 0.01$ MeV, with the right set [(d)-(f)] for $\varepsilon_b = 2.03$ MeV.

which appears in Eq.(4). The nuclear breakup dynamics require that $\delta_R(\varepsilon_b) \rightarrow 0$, as ε_b increases, implying that $R_n \rightarrow R_0$, due to the short-range nature of nuclear forces. However, as $\varepsilon_b \rightarrow 0$, $\delta_R(\varepsilon_b)$ increases and so does R_n , leading to a significant nuclear effect in the peripheral region. Therefore, the function $\delta_R(\varepsilon_b)$ is introduced to take into account the well-known effect which occurs in weakly-bound systems, as in halo nuclei, in which the nuclear forces are stretched beyond the usual range.

Quantitatively, since this ${}^8\text{Li}+{}^{208}\text{Pb}$ reaction is Coulomb-dominated, we observe that at forward angles both $d\sigma_{tot}/d\Omega$ and $d\sigma_{Coul}/d\Omega$ are substantially larger than $d\sigma_{nucl}/d\Omega$ (about three orders of magnitude as ε_b decreases). A further inspection of this figure shows that for $E_{lab} = 60$ MeV, we notice that the total and Coulomb breakup cross sections are more similar compared to $E_{lab} = 36$ MeV, with the difference coming from the competition between the nuclear and Coulomb interactions above the barrier (for a discussion on the role of the diagonal Coulomb interaction, see also Ref. [22]).

In order to better elucidate the importance of the nuclear absorption in the breakup process, we present in Fig. 7, for the ${}^8\text{Li}+{}^{208}\text{Pb}$ reaction, the integrated total breakup cross section as well as the total fusion cross sections as functions of ε_b . In this regard, we are extending

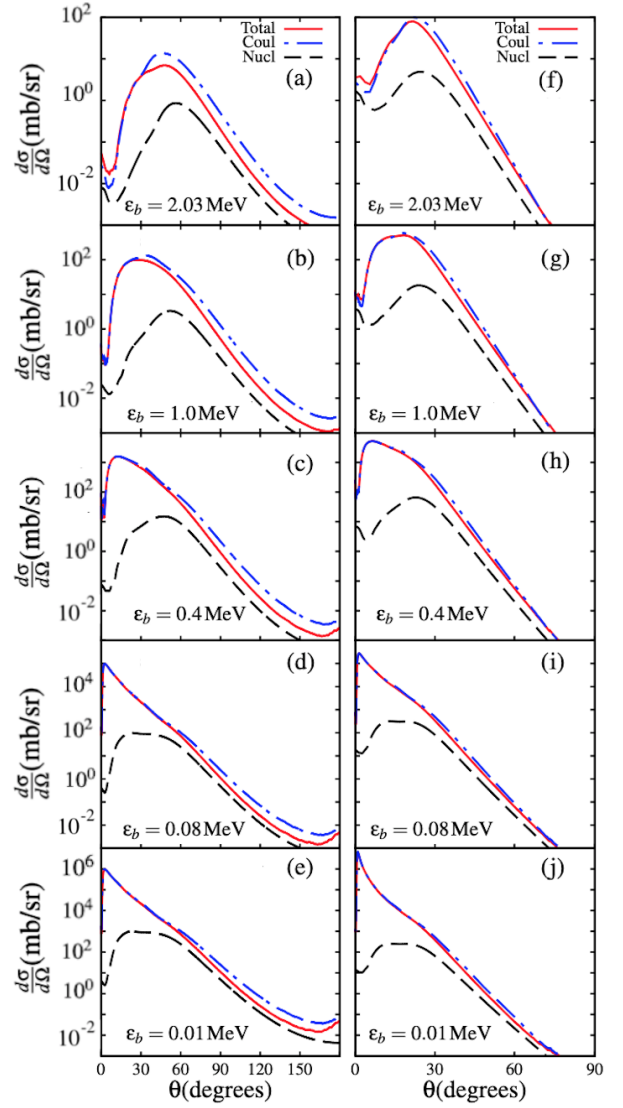


FIG. 6: For incident energies $E_{lab} = 36$ MeV (left column) and $E_{lab} = 60$ MeV (right column), with fixed different ε_b (shown inside the panels), the ${}^8\text{Li}+{}^{208}\text{Pb}$ angular distributions for the total, Coulomb and nuclear $d\sigma/d\Omega$ (identified in the upper panels) are shown as functions of the c.m. angle θ .

a previous analysis done for this reaction in Ref. [37], in which the total fusion cross sections are shown as functions of the incident energy for different projectile binding energies. The breakup cross section obtained in the presence of nuclear absorption (i.e., $W_{ct}^{nucl} \neq 0$, $W_{nt}^{nucl} \neq 0$), are indicated by the label “BU”. The breakup cross section obtained in the absence of nuclear absorption (i.e., $W_{ct} = W_{nt} = 0$), are indicated by “NA”. The total fusion cross section is labeled as “TF”. By observing this figure, it follows that, as $\varepsilon_b \rightarrow 2.03$ MeV, the nuclear absorption contributes to largely reduce the breakup cross section about one order magnitude in the log-scale. However, we observe that the nu-

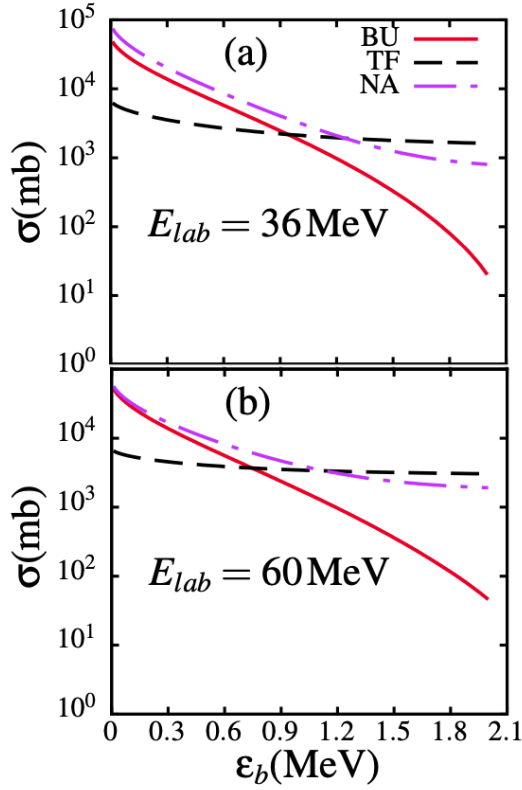


FIG. 7: For the ${}^8\text{Li}+{}^{208}\text{Pb}$ reaction, by considering $E_{lab}=36$ MeV (a) and 60 MeV (b), it is shown the integrated breakup cross sections (BU) (when both W_{ct}^{nucl} and W_{nt}^{nucl} are contributing), the breakup cross section without absorption (NA) (when $W_{ct}^{nucl} = W_{nt}^{nucl} = 0$), and the total fusion cross section (TF), as functions of the projectile binding energy ϵ_b .

clear absorption plays a minor role on the breakup cross section for smaller binding energies, being negligible for $\epsilon_b \rightarrow 0.01$ MeV, in particular at $E_{lab} = 60$ MeV. In this case, $\sigma_{NA} \simeq \sigma_{BU} \gg \sigma_{TF}$, (where σ_{BU} is the breakup cross section followed by fragments absorption, and σ_{NA} is the breakup cross section without fragments absorption after breakup). A larger breakup cross section over the total fusion cross section can be understood as due to the fact that, when the breakup occurs where classically the trajectory is far away from the target, the projectile fragments have no easy access to the absorption region, thus significantly reducing the flux that contributes to the fusion cross section. However, as expected, as $\epsilon_b \rightarrow 2.03$ MeV, where the breakup process occurs closer to the target, where the probability for the projectile fragments to survive absorption is significantly reduced, we observe that $\sigma_{BU} \ll \sigma_{NA} < \sigma_{TF}$. A weak dependence of the total fusion cross section on the binding energy compared to the breakup cross section is also observed. The energy region well above the Coulomb barrier is particularly dominated by the complete fusion process. As shown in Ref. [35], the complete fusion cross section is in-

significantly dependent on the projectile ϵ_b for ${}^7\text{Li}+{}^{209}\text{Bi}$ reaction. We believe that these observations would be valid for any loosely bound projectile, and hence there is nothing unusual in the breakup of the ${}^8\text{Li}$ nucleus.

Concerning our approach to total fusion (TF) and absorption, let us clarify that: In the standard CDCC method, the optical potentials are chosen to describe the elastic scattering of the fragments by the target. So, their imaginary parts account for the absorption to fusion and other direct channels (surface reactions). Nevertheless, as direct reaction cross sections are expected to be small for the interactions between fragments and targets selected in this work, the TF cross section provides the major contribution to this absorption.

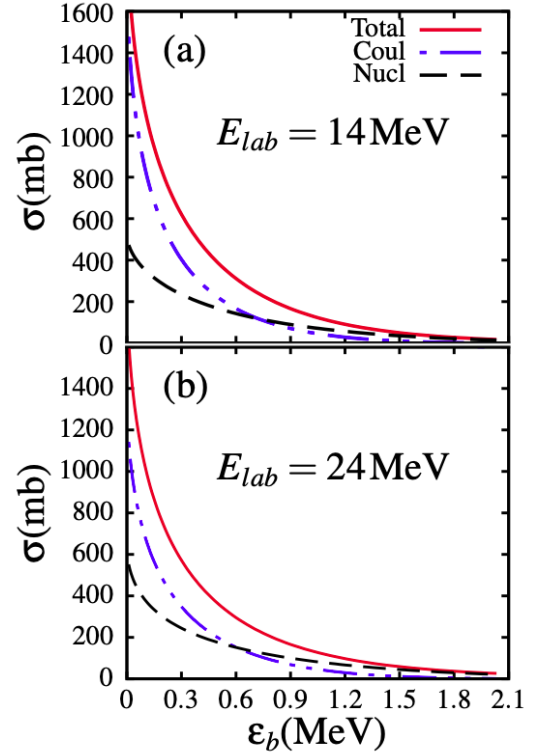


FIG. 8: For the ${}^8\text{Li}+{}^{12}\text{C}$ breakup reaction, the angular-integrated total, Coulomb and nuclear breakup cross sections are given as functions of the projectile binding energy ϵ_b , for the incident energies $E_{lab}=14$ MeV (a) and 24 MeV (b).

For a better quantitative assessment of these results, we consider the integrated total (σ_{tot}), Coulomb (σ_{Coul}), and nuclear (σ_{nucl}) breakup cross sections, which are displayed as functions of ϵ_b in Fig. 8 (for the ${}^{12}\text{C}$ target), and in Fig. 9 (for the ${}^{208}\text{Pb}$ target). The results in both figures confirm the conclusions already drawn from Figs. 4 and 6. For example, both panels of Fig. 8, show that as $\epsilon_b \rightarrow 0.01$ MeV, $\sigma_{Coul} > \sigma_{nucl}$ ($\sigma_{Coul} \simeq \sigma_{tot}$), whereas $\sigma_{Coul} < \sigma_{nucl} \simeq \sigma_{tot}$ ($\sigma_{nucl} \simeq \sigma_{tot}$) as $\epsilon_b \rightarrow 2.03$ MeV. For ${}^{208}\text{Pb}$ target, the results are shown in the presence of nuclear absorption. When the nuclear absorp-

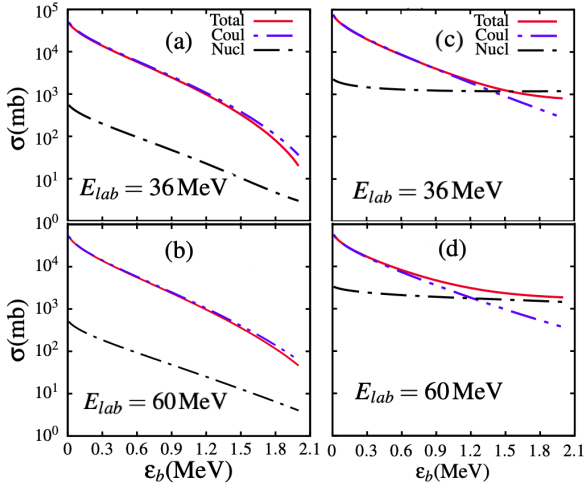


FIG. 9: The angular-integrated total, Coulomb and nuclear breakup cross sections are given for the ${}^8\text{Li}+{}^{208}\text{Pb}$ breakup reaction as functions of ε_b , with nuclear absorption in the panels (a) and (b); and without absorption in the panels (c) and (d). As indicated, the incident energies are $E_{lab}=36$ MeV [panels (a) and (c)] and 60 MeV [panels (b) and (d)].

tion is taken into account [panels (a) and (b)], we notice that $\sigma_{coul} \simeq \sigma_{tot} \gg \sigma_{nucl}$ and this is independent of ε_b . In the absence of the nuclear absorption [panels (c) and (d)], while $\sigma_{coul} \simeq \sigma_{tot} \gg \sigma_{nucl}$ remains valid for $\varepsilon_b \rightarrow 0.01$ MeV, it is noticed that $\sigma_{tot} \simeq \sigma_{nucl} > \sigma_{Coul}$, for $\varepsilon_b \rightarrow 2.03$ MeV, which further highlights the importance of the nuclear absorption for large binding energies. The results in this figure further support the fact that strong nuclear absorption in the inner region is the main factor that dictates the importance of the Coulomb breakup cross section over its nuclear counterparts. In Table III, we provide more quantitative results, given as fractions from σ_{tot} and σ_{nucl} , reflecting the competition between the different cross sections, by selecting the two limiting binding energies we are studying, i.e., $\varepsilon_b = 0.01$ MeV and $\varepsilon_b = 2.03$ MeV. We are also including σ_{int} , as defined by

$$\sigma_{int} = \sigma_{tot} - (\sigma_{Coul} + \sigma_{nucl}), \quad (9)$$

which we naively regard as the Coulomb-nuclear interference and that will be discussed in the next subsection. From this table, it becomes evident that, when ε_b decreases, σ_{Coul} (approaching to σ_{tot}) becomes substantially larger than σ_{nucl} . Also, for the light ${}^{12}\text{C}$ target, at $E_{lab} = 14$ MeV and 24 MeV, we note that $\sigma_{Coul}/\sigma_{nucl}$ rapidly grows, when varying ε_b from 2.03 MeV down to 0.01 MeV. As shown, in this energy interval, $\sigma_{Coul}/\sigma_{nucl}$ increases from 0.03 to 3.12 for 14 MeV, and from 0.06 to 2.10 for 24 MeV. This indicates that, as the binding energy decreases, the ${}^8\text{Li}+{}^{12}\text{C}$ reaction becomes like a “Coulomb-dominated reaction”, with the emergence of a long-range behavior. Moreover, with the heavy tar-

get at $E_{lab} = 36$ MeV, in the presence of nuclear absorption, for $\varepsilon_b = 2.03$ MeV, $\sigma_{coul}/\sigma_{nucl} = 12$, whereas $\sigma_{coul}/\sigma_{nucl} \simeq 90$ for $\varepsilon_b = 0.01$ MeV. It is noticed in this case that this ratio is substantially affected in the absence of nuclear absorption (NA), becoming $\sigma_{coul}/\sigma_{nucl} \simeq 0.06$ ($\varepsilon_b = 2.03$ MeV), and $\sigma_{coul}/\sigma_{nucl} \simeq 34$ ($\varepsilon_b = 0.01$ MeV).

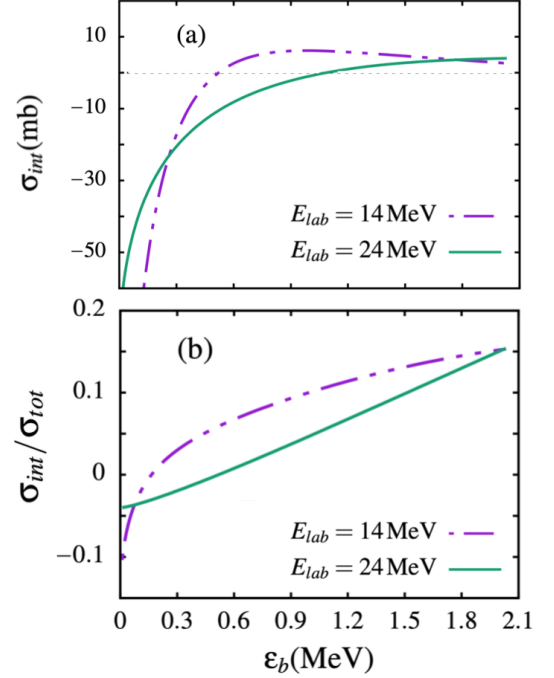


FIG. 10: The ${}^8\text{Li}+{}^{12}\text{C}$ integrated Coulomb-nuclear interference σ_{int} [panel (a)], given by (9), with the respective ratio $\sigma_{int}/\sigma_{tot}$ [panel (b)], are shown as functions of ε_b , for the colliding energies $E_{lab} = 14$ and 24 MeV.

C. Coulomb-nuclear interference

It is well-known that the incoherent sum of the Coulomb and nuclear breakup cross section ($\sigma_{Coul} + \sigma_{nucl}$) is always different from their coherent sum, σ_{tot} , due to the Coulomb-nuclear interference effect. To assess this effect in the context of very weak ground-state binding energy, we consider σ_{int} as defined in Eq. (9) to estimate the Coulomb-nuclear interference. Given that, for the two limiting binding energies, the quantitative results for σ_{int} are already furnished in Table III as ratios with respect to σ_{tot} and σ_{nucl} . In Figs. 10 and 11 (respectively, for ${}^{12}\text{C}$ and ${}^{208}\text{Pb}$ targets), we provide the exact σ_{int} behaviors, together with their respective ratios $\sigma_{int}/\sigma_{tot}$, as functions of ε_b , in a way to clarify that the differences between σ_{tot} and $(\sigma_{Coul} + \sigma_{nucl})$ are quite large in both the cases, with the amount varying with E_{lab} ($|\sigma_{int}|$ decreasing with increasing E_{lab}). The Coulomb-nuclear interference is strongly dependent on ε_b . As one can no-

TABLE III: Coulomb, nuclear and interference cross-sections for the ${}^8\text{Li} + {}^{12}\text{C}$ and ${}^8\text{Li} + {}^{208}\text{Pb}$, considering $n-{}^7\text{Li}$ binding energies $\varepsilon_b = 0.01$ MeV and 2.03 MeV. For each target, we present our results, in terms of ratios, for two colliding energies. For ${}^{208}\text{Pb}$ target, with no-nuclear absorption (NA) the results are shown within parenthesis below the ones with absorption.

Target	E_{lab} (MeV)	$\varepsilon_b = 2.03$ MeV					$\varepsilon_b = 0.01$ MeV				
		$\frac{\sigma_{Coul}}{\sigma_{tot}}$	$\frac{\sigma_{nucl}}{\sigma_{tot}}$	$\frac{\sigma_{Coul}}{\sigma_{nucl}}$	$\frac{\sigma_{int}}{\sigma_{nucl}}$	$\frac{\sigma_{int}}{\sigma_{tot}}$	$\frac{\sigma_{Coul}}{\sigma_{tot}}$	$\frac{\sigma_{nucl}}{\sigma_{tot}}$	$\frac{\sigma_{Coul}}{\sigma_{nucl}}$	$\frac{\sigma_{int}}{\sigma_{nucl}}$	$\frac{\sigma_{int}}{\sigma_{tot}}$
${}^{12}\text{C}$	14	0.024	0.824	0.029	0.186	0.153	0.836	0.268	3.123	-0.387	-0.104
	24	0.048	0.808	0.059	0.190	0.154	0.701	0.339	2.069	-0.118	-0.040
${}^{208}\text{Pb}$	36	1.800	0.150	12.00	-6.333	-0.950	1.033	0.012	90.16	-3.850	-0.044
		(0.344)	(1.481)	(0.232)	(-0.557)	(-0.825)	(1.032)	(0.029)	(33.97)	(-2.061)	(-0.063)
	60	1.326	0.087	15.25	-4.750	-0.413	1.015	0.010	104.6	-2.540	-0.025
		(0.198)	(0.783)	(0.253)	(0.025)	(0.019)	(1.000)	(0.059)	(17.03)	(-0.991)	(-0.058)

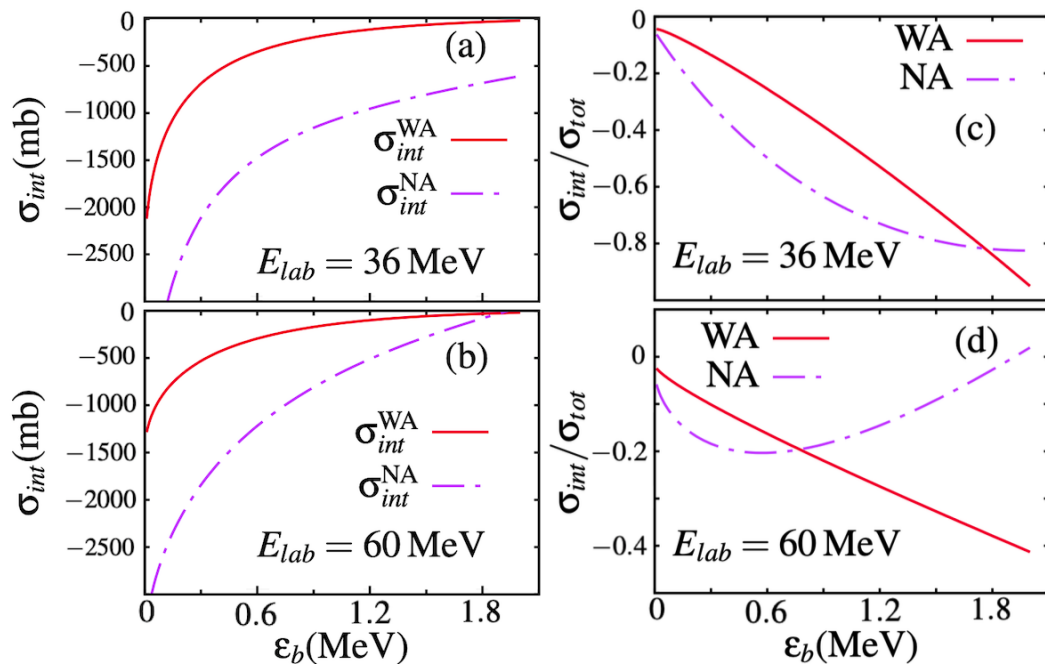


FIG. 11: The ${}^8\text{Li} + {}^{208}\text{Pb}$ integrated Coulomb-nuclear interference σ_{int} [panels (a) and (b)], given by (9), with their ratios $\sigma_{int}/\sigma_{tot}$ [panels (c) and (d)], are shown as functions of ε_b , for $E_{lab} = 36$ and 60 MeV (upper and lower frames, respectively). σ_{int}^{WA} (solid lines) denotes the interference when the breakup is followed by nuclear absorption, with σ_{int}^{NA} (dot-dashed lines) denoting interference with no nuclear absorption.

tice, it appears to increase as ε_b decreases, and becomes quite small as $\varepsilon_b \rightarrow 2.03$ MeV.

For the ${}^8\text{Li} + {}^{208}\text{Pb}$ reaction, nuclear absorption which is already shown to reduce the breakup cross section (Fig.7), is expected to be more relevant on the Coulomb-nuclear interference. The Coulomb-nuclear interference obtained when the breakup is followed by nuclear absorption (i.e., $W_{ct}^{nucl} \neq 0$, $W_{nt}^{nucl} \neq 0$), is denoted by σ_{int}^{WA} (WA standing for “with absorption”), and by σ_{int}^{NA} the Coulomb-nuclear interference obtained when $W_{ct}^{nucl} = W_{nt}^{nucl} = 0$. Therefore, in order to assess the relevance of the nuclear absorption on this interference, we compare σ_{int}^{WA} with σ_{int}^{NA} . The results are presented in Fig.11. In

this figure, the panels (a) and (b) are for the exact σ_{int} results, whereas in panels (c) and (d) we have the respective ratios $\sigma_{int}/\sigma_{tot}$. The upper panels are for $E_{lab} = 36$ MeV, and the lower panels for $E_{lab} = 60$ MeV. The absorption contribution to σ_{int} is verified by the observed difference $|\sigma_{int}^{NA} - \sigma_{int}^{WA}|$, which are clearly shown for both E_{lab} energies, as ε_b varies.

Besides the fact that the Coulomb-nuclear interference is shown to be larger in the very small binding energy limits, such larger values may also be influenced by the large magnitudes of the total and Coulomb breakup cross sections, which are shown in Figs. 9 and 10. However, as verified from Table III, the ratios $\sigma_{Coul}/\sigma_{tot}$ for the

smaller binding are enough deviating from one (when full absorption is considered, in the ^{208}Pb case). Consistently, we also noticed from the results given in Table III, that $\sigma_{int}/\sigma_{tot}$ is larger for $\varepsilon_b = 2.03\text{ MeV}$ when we have the usual cross section values with absorption. Further investigation may be required to clarify the ε_b dependence of Coulomb-nuclear interference, in support to the actual results that are shown an overall significant effect of nuclear absorption.

In the case of such weakly-bound projectiles, a better understanding of the function $\delta_R(\varepsilon_b)$, which appears in Eq.(4), could shed more light on the complexity of the Coulomb-nuclear interference. In such cases, R_n can significantly deviate from R_0 , since the nuclear breakup dynamics requires that $\delta_R(\varepsilon_b) \rightarrow 0$ for larger values of ε_b . Particularly, the main characteristics of this function could show up in a study with charged projectiles, considering that strong Coulomb/nuclear interference has been observed for the reaction of proton halo ^8B with ^{58}Ni target [6, 8, 11, 58], in which we have a very weakly-bound projectile with breakup threshold of 0.137 MeV .

IV. CONCLUSION

We have presented a study on the breakup of the weakly-bound ^8Li ($n-^7\text{Li}$) projectile on light and heavy target masses, namely, ^{12}C and ^{208}Pb . Our main objective was to investigate the dependence of the total, Coulomb and nuclear breakup cross sections, on the ^8Li ground-state binding energy ε_b , in order to study the peripherality of the total, Coulomb and nuclear breakup processes, which are associated to the weaker binding energy of the projectile. To this end, apart from the experimentally-known ground-state binding energy of the $n-^7\text{Li}$ system, we artificially considered four other binding energies, below the experimental value, down to $\varepsilon_b = 0.01\text{ MeV}$, which is much smaller than the experimental value, $\varepsilon_b = 2.03\text{ MeV}$. From our analysis it is shown that the total, Coulomb and nuclear breakup processes become peripheral as $\varepsilon_b \rightarrow 0.01\text{ MeV}$, regardless the target mass. We argue that the peripherality of the nuclear breakup in this case is primarily related to

the spacial extension of the corresponding ground-state wave function, which is related to weaker binding energy. The peripheral region is determined by the range of the nuclear forces R_0 , and the corresponding extension of the ground-state wave function, which is associated to a function $\delta_R(\varepsilon_b)$, expressed by R_n defined in Eq. (4). By taking into account the fact that close to the n -core $\varepsilon_b \rightarrow 0$ limit, a long-range interaction is expected to emerge between projectile and target (similar as for three-body halo-nuclei systems [59]), the size of the associated wave function will increase significantly in this limit. So, a detailed investigation of this function $\delta_R(\varepsilon_b)$ (which should go to zero by increasing ε_b) can shed more light into the dynamics of nuclear breakups induced by loosely bound projectiles. It is also noticed that the variation of ε_b strongly affects the Coulomb breakup, as compared to the nuclear breakup, such that as $\varepsilon_b \rightarrow 0.01\text{ MeV}$, the Coulomb breakup becomes dominant even for the ^{12}C target, which is known to be naturally dominated by nuclear breakup. Therefore, in view of this binding-energy dependence, one may infer that the expression “naturally-dominated by nuclear breakup” may be relative to the projectile binding energy. It is also verified that the nuclear absorption has an insignificant effect on the total and nuclear breakup cross sections when decreasing the binding energy to small binding such as $\varepsilon_b \rightarrow 0.01\text{ MeV}$. In this small binding energy region, we found that the total breakup cross section is larger than the calculated total fusion cross section, while as expected, the opposite is observed as $\varepsilon_b \rightarrow 2.03\text{ MeV}$.

Acknowledgements

We thank T. Frederico, B.V. Carlson and L. F. Canto for useful discussions. B.M. is also grateful to the South American Institute of Fundamental Research (ICTP-SAIFR) for local facilities. For partial support, we also thank Conselho Nacional de Desenvolvimento Científico e Tecnológico [INCT-FNA Proc.464898/2014-5 (LT and JL), Proc. 304469/2019-0(LT) and Proc. 306652/2017-0(JL)], and Fundação de Amparo à Pesquisa do Estado de São Paulo [Projs. 2017/05660-0(LT)].

-
- [1] Y. Suzuki, K. Yabana, R.G. Lovas, K. Varga, *Structure and Reactions of Light Exotic Nuclei* (Taylor & Francis Group, London and New York, 2003).
 - [2] I. J. Thompson and F. M. Nunes, *Nuclear Reactions for Astrophysics* (Cambridge University Press, New York, 2009).
 - [3] R. Chatterjee and R. Shyam, Prog. Part. Nucl. Phys. **103**, 67 (2018).
 - [4] F. M. Nunes and I. J. Thompson, Phys. Rev. C **57**, R2818 (1998).
 - [5] F. M. Nunes and I. J. Thompson, Phys. Rev. C **59**, 2652 (1999).
 - [6] J. Margueron, A. Bonaccorso, and D. M. Brink, Nucl. Phys. A **703**, 105 (2002).
 - [7] P. Capel, D. Baye and V. S. Melezhik, Phys. Rev. C **68**, 014612 (2003).
 - [8] T. Tarutina and M. S. Hussein, Phys. Rev. C **70**, 034603 (2004).
 - [9] M. S. Hussein, R. Lichtenthaler, F. M. Nunes and I. J. Thompson, Phys. Lett. B **640**, 91 (2006).
 - [10] L. F. Canto, P. R. S. Gomes, R. Donangelo, and M. S. Hussein, Phys. Rep. **424**, 1 (2006).
 - [11] J. Lubian, T. Correa, E. F. Aguilera, L. F. Canto, A. Gomez-Camacho, E. M. Quiroz, and P. R. S. Gomes,

- Phys. Rev. C **79**, 064605 (2009).
- [12] L. F. Canto, J. Lubian, P. R. S. Gomes, and M. S. Hussein, Phys. Rev. C **80**, 047601 (2009).
 - [13] Y. Kucuk and A. M. Moro, Phys. Rev. C **86**, 034601 (2012).
 - [14] P. Capel, J. Phys. G: Nucl. Part. Phys. **41**, 094002 (2014).
 - [15] D. R. Otomar, P. R. S. Gomes, J. Lubian, L. F. Canto and M. S. Hussein, Phys. Rev. C **87**, 014615 (2013).
 - [16] D. R. Otomar, P. R. S. Gomes, J. Lubian, L. F. Canto and M. S. Hussein, Phys. Rev. C **92**, 064609 (2015).
 - [17] B. Mukeru, M. L. Lekala and A. S. Denikin, J. Phys. G: Nucl. Part. Phys. **42**, 015109 (2015).
 - [18] B. Mukeru and M. L. Lekala, Phys. Rev. C **91**, 064609 (2015).
 - [19] S. G. Manjeet, Chin. Phys. C **40**, 054101 (2016).
 - [20] P. Descouvemont, L.F. Canto, M.S. Hussein, Phys. Rev. C **95**, 014604 (2017).
 - [21] B. Mukeru and M.L. Lekala, Int. J. Mod. Phys. E **26**, 1750075 (2017).
 - [22] B. Mukeru, T. Frederico, and L. Tomio, Phys. Rev. C **102**, 064623 (2020).
 - [23] T. Nakamura, N. Kobayashi, Y. Kondo, Y. Satou, N. Aoi, H. Baba, et al., Phys. Rev. Lett. **103**, 262501 (2009).
 - [24] C. Nociforo et al., Phys. Lett. B **605**, 79 (2005).
 - [25] T. Aumann and T. Nakamura, Phys. Scr. T **152**, 014012 (2013).
 - [26] N. Fukuda, T. Nakamura, N. Aoi, N. Imai, M. Ishihara, T. Kobayashi, H. Iwasaki, T. Kubo, A. Mengoni, M. Notani, H. Otsu, H. Sakurai, S. Shimoura, T. Teranishi, Y. X. Watanabe, K. Yoneda, Phys. Rev. C **70**, 054606 (2004).
 - [27] B. Abu-Ibrahim and Y. Suzuki, Progr. Theor. Phys. **112**, 1013 (2004).
 - [28] C. A. Bertulani and G. Baur, Phys. Rep. **163**, 299 (1988).
 - [29] A. Winther and K. Alder, Nucl. Phys. A **319**, 518 (1979).
 - [30] G. Baur, K. Hencken, and D. Trautmann, Prog. Part. Nucl. Phys. **51**, 487 (2003).
 - [31] G. Baur and H. Rebel, Annu. Rev. Nucl. Part. Sci. **46**, 321 (1996).
 - [32] B. Wang, W. J. Zhao, P. R. S. Gomes, E. G. Zhao, and S.-G. Zhou, Phys. Rev. C **90**, 034612 (2014).
 - [33] P. K. Rath, S. Santra, N. L. Singh, R. Tripathi, V. V. Parkar, B. K. Nayak, K. Mahata, R. Palit, S. Kumar, S. Mukherjee, S. Appannababu, R. K. Choudhury, Phys. Rev. C **79**, 051601(R) (2009).
 - [34] J. Rangel, J. Lubian, L. F. Canto, and P. R. S. Gomes, Phys. Rev. C **93**, 054610 (2016).
 - [35] J. Lei A. M. Moro, Phys. Rev. Lett. **122**, 042503 (2019).
 - [36] B. Mukeru, J. Phys. G: Nucl. Part. Phys. **45**, 065201 (2018).
 - [37] B. Mukeru, M.L. Lekala, J. Lubian and L. Tomio, Nucl. Phys. A **996**, 121700 (2020).
 - [38] V. Jha, V. V. Parkar and S. Kailas, Phys. Rep. **845** 1 (2020).
 - [39] K. J. Cook, I. P. Carter, E. C. Simpson, M. Dasgupta, D. J. Hinde, L. T. Bezzina, S. Kalkal, C. Sengupta, C. Simenel, B. M. A. Swinton-Bland, K. Vo-Phuoc, E. Williams, Phys. Rev. C **97** 021601(R) (2018).
 - [40] A. Pakou et al., Eur. Phys. J. A **51**, 55 (2015).
 - [41] V. Guimarães, J. Lubian, J. J. Kolata, E. F. Aguilera, M. Assunção, V. Morcelle, Eur. Phys. J. A **54**, 223 (2018).
 - [42] M. Wang, et al., Chin. Phys. C **41**, 030003 (2017). [See also at <https://www.nndc.bnl.gov/nudat2/>].
 - [43] N. Austern et al., Phys. Rep. **154**, 125 (1987).
 - [44] I. J. Thompson, Comput. Phys. Rep. **7**, 167 (1988).
 - [45] L. F. Canto, P. R. S. Gomes, R. Donangelo, J. Lubian and M. S. Hussein, Phys. Rep. **596**, 1 (2015).
 - [46] M. Abramowitz and I. Stegun, *Handbook of Mathematical Functions: with Formulas, Graphs, and Mathematical Tables* (Dover Publications, National Bureau of Standards, New York, 1964).
 - [47] L. F. Canto and M. S. Hussein, *Scattering theory of molecules, atoms and nuclei* (World Scientific Publishing Co. Pte. Ltd, Singapore, 2013)
 - [48] C. A. Bertulani, *Comput. Phys. Commun.* **156**, 123 (2003).
 - [49] A. M. Moro, R. Crespo, H. Garcia-Martinez, E. F. Aguilera, E. Martinez-Quiroz, J. Gomez-Camacho, F. M. Nunes, Phys. Rev. C **68**, 034614 (2003).
 - [50] G. W. Fan, M. Fukuda, D. Nishimura, X. L. Cai, S. Fukuda, I. Hachiuma, et al., Phys. Rev. C **91**, 014614 (2015).
 - [51] I. Tanihata, T. Kobayashi, O. Yamakawa, S. Shimoura, K. Ekuni, K. Sugimoto, N. Takahashi, T. Shimoda, H. Sato, Phys. Lett. B **206**, 592 (1988).
 - [52] A. Barioni, V. Guimarães, A. Lépine-Szily, R. Lichtenthäler, D. R. Mendes, E. Crema, K. C. C. Pires, M.C. Morais, V. Morcelle, P. N. deFaria, R. P. Condori., A. M. Moro., D. S. Monteiro, J. M. B. Shorto, J. Lubian, M. Assunção, Phys. Rev. C **80**, 034617 (2009).
 - [53] J. Cook, Nucl. Phys. A **388**, 153 (1982).
 - [54] A. J. Koning and J. P. Delaroche, Nucl. Phys. A **713**, 231 (2003).
 - [55] F. D. Becchetti, W. Z. Liu, K. Ashktorab, J. F. Bajema, J. A. Brown, J. W. Janecke, D. A. Roberts, J. J. Kolata, K. L. Lamkin, A. Morsad, R. J. Smith, X. J. Kong, R. E. Warner, Phys. Rev. C **48**, 308 (1993).
 - [56] A. V. Karpov, A. S. Denikin, A. P. Alekseev, V. I. Zagrebaev, V. A. Rachkov, M. A. Naumenko, and V. V. Saiko, Phys. Atom. Nucl. **79**, 749 (2016) and <http://nrv.jinr.ru/nrv/webnrv/expdata> database.
 - [57] J. J. Kolata, V. Z. Goldberg, L. O. Lamm, M. G. Marino, C. J. O'Keeffe, G. Rogachev, et al., Phys. Rev. C **65**, 054616 (2002).
 - [58] J. A. Tostevin, F. M. Nunes, and I. J. Thompson, Phys. Rev. C **63**, 024617 (2001).
 - [59] T. Frederico, A. Delfino, L. Tomio and M.T. Yamashita, Prog. Part. Nucl. Phys. **67**, 939 (2012).